Position-Dependent Multibody Dynamic Modeling of Machine Tools Based on Improved Reduced Order Models

Mohit Law
Ph.D. Candidate

A. Srikantha Phani
Assistant Professor

Yusuf Altintas
Professor
Fellow ASME
e-mail: altintas@mech.ubc.ca

Department of Mechanical Engineering,
The University of British Columbia,
2054-6250 Applied Science Lane,
Vancouver, BC, V6T 1Z4, Canada

Dynamic response of a machine tool structure varies along the tool path depending on the changes in its structural configurations. The productivity of the machine tool varies as a function of its frequency response function (FRF) which determines its chatter stability and productivity. This paper presents a computationally efficient reduced order model to obtain the FRF at the tool center point of a machine tool at any desired position within its work volume. The machine tool is represented by its position invariant substructures. These substructures are assembled at the contacting interfaces by using novel adaptations of constraint formulations. As the tool moves to a new position, these constraint equations are updated to predict the FRFs efficiently without having to use computationally costly full order finite element or modal models. To facilitate dynamic substructuring, an improved variant of standard component mode synthesis method is developed which automates reduced order determination by retaining only the important modes of the subsystems. Position-dependent dynamic behavior and chatter stability charts are successfully simulated for a virtual three axis milling machine, using the substructurally synthesized reduced order model. Stability lobes obtained using the reduced order model agree well with the corresponding full-order system. [DOI: 10.1115/1.4023453]

Keywords: machine tools, finite element, model reduction, substructuring, dynamics, stability

1 Introduction

Lack of sufficient dynamic stiffness at the tool center point (TCP) may lead to a regenerative chatter vibration which is detrimental to the performance and integrity of entire machine tool system, resulting in: poor surface quality; accelerated tool wear; damage of work piece and machine structural elements; and, ultimately limiting productivity [1]. Machine tool stability is governed both by the tool-tool holder-spindle characteristics and by the modal properties, i.e., the eigenfrequencies and mode shapes of the machine tool structural elements. These modal properties in turn are a function of the instantaneous position of machine structural elements within the machine work volume. Experimental procedures called as "acceptance tests" [2] are usually employed to obtain the position-dependent behavior of machine tools that are already built.

An alternate approach in place of costly and time consuming physical prototyping and testing, is to evaluate the position-dependent response based on finite element (FE) models of machine tools [3]. FE models have very large order, typically 1,000,000 degrees of freedom (DOFs) or more for a typical three axis machine tool. Dynamic response analyses at discrete positions for such large order models require cumbersome adaptive/re-meshing meshing strategies to account for the position-varying boundary conditions. Recent trends are to treat this class of problems using co-simulation with FE solvers coupled to standard flexible multibody dynamic analysis software [4,5]. These co-simulations are time prohibitive, and are restricted to flexible bodies attached at geometrically fixed contact points, hence not suitable for flexible machine tool structural elements undergoing relative motion; which consist of multiple geometrically changing contact points that change as the tool moves from one position to another.

Contributed by the Manufacturing Engineering Division of ASME for publication in the Journal of Manufacturing Science and Engineering. Manuscript received January 31, 2012; final manuscript received October 19, 2012; published online March 22, 2013. Assoc. Editor: Tony Schmitz.

Other methods related to modeling of systems with position-dependent dynamics have largely centered on reducing the moving contact problem to that of a rigid body in contact with and moving over a flexible body with uniform nodal spacing [6,7]. An alternate comprehensive modeling scheme to evaluate machine tool response at discrete positions for control system design was proposed by Fonseca in Ref. [8].

To facilitate a computationally efficient modeling alternative to model position-dependency of machine tools in place of the presently used time consuming full FE models by the designers, a bottom-up approach based on substructural synthesis of flexible reduced models is followed in this paper. The substructural synthesis is akin to a generic component mode synthesis (CMS) approach. Each substructure modeled with FE is reduced to be represented by a set of interface (exterior) DOFs complemented by a set of generalized (modal) DOFs corresponding to the interior DOFs.

For reduced models to have a manageable size, while retaining the essential dynamic characteristics of the full model, a major challenge with the CMS approach is to identify the number of mode sets from the individual components to be retained. Usually, either the first few low frequency modes; or modes with an eigenfrequency up to 1.5–2 times the maximum excitation frequency are retained [9]; this however may increase the size of the reduced model. Moreover, it may not be sufficient to represent the flexibilities of substructures using only a single mode set for each component due to their position-varying boundary conditions [7]. An accurate representation of the full frequency spectrum while retaining computational efficiency requires answering the following question: *how many and which modes of the subsystem need to be retained?*

Modal methods of mode selection [10,11] based on "dominance measures" require converting the large scale second order ordinary differential equations obtained from the FE model to a linear first order state-space model, resulting in even larger system matrices. Other methods [9,12,13] sort and retain the most significant

modes based on the strength of interaction between the subsystem and the main system. Their main concern however, was not the dynamical substructural system, but its effect on the main system. A mode selection criterion was also proposed by Park in Ref. [14]. While being reliably able to select important modes, their top–down approach was based on partitioning of continuums into substructures, resulting in a conforming mesh at the interfaces. Hence, is different than the generalized bottom-up approach followed in this work, such as to synthesize substructures which may have been modeled separately and may have nonconforming mesh distribution at their interfaces. Alternatively, suitable subspace dimension determination may be carried out using an adaptive refinement method as in Ref. [15], wherein modes were included/excluded iteratively from each subspace depending upon how posteriori error estimates of each CMS subspace influenced the error in the synthesized reduced model. Though automated, it is computationally expensive and inefficient.

Position-dependency in this work is modeled by synthesizing reduced substructures whose response is position-independent. Reduced substructural models which represent higher order dynamics while keeping the order to a minimum are developed using a novel mode indicator based identification criterion which identifies significant modes as those simulated from a frequency response function (FRF) constructed between the most controllable and observable locations within the subset of the interior DOFs. Furthermore, a generalized framework tolerating mesh incompatibility at substructural interfaces is presented by describing displacement compatibility between adjacent substructures with sets of algebraic equations, which are updated to account for relative motion; thereby simulating the position-dependent response.

The organization of this paper is summarized in Fig. 1. At first, generalized modeling of position-dependent dynamics based on substructural assembly is presented in Sec. 2; followed by improved reduced order modeling in Sec. 3. In Sec. 4, a three axis Cartesian milling machine is used to demonstrate the modeling of the position-dependent behavior based on improved reduced order models. The effects of position-dependent structural dynamics on the chatter stability of milling operations are presented in Sec. 5. The paper is concluded in Sec. 6.

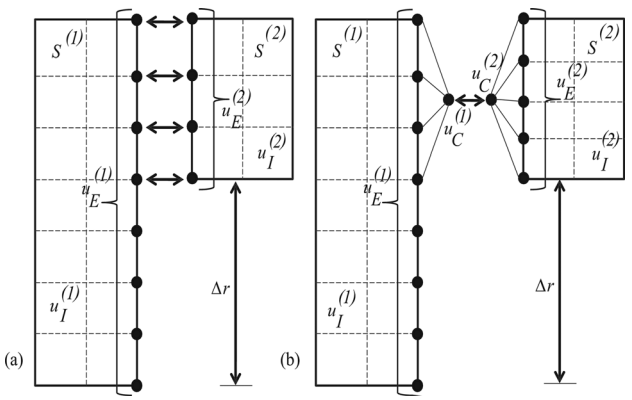

Fig. 2 Substructural assembly by enforcing continuity constraints, (*a*) compatible substructures, (*b*) incompatible substructures

2 Generalized Substructural Formulation for Position-Dependency

Machine tools may be treated as an assembly of flexible multibodies modeled as substructural components using FE. Main substructural components of a machine tool are: column, bed, table, spindle, and feed drives. The objective of generalized formulation is to predict the dynamic response of the complete machine efficiently as one component changes its position relative to others.

2.1 Assembling Substructural Models. Consider two substructures $S^{(1)}$ and $S^{(2)}$ as shown in Fig. 2; which may represent any of the machine components with relative motion between them. The displacement vector $\boldsymbol{u}^{(n)}$ for substructure n $(n=1,2)$ consists of displacements at the interior DOFs $\boldsymbol{u}_{\mathrm{I}}^{(n)}$, and at the exterior (interface) DOFs $\boldsymbol{u}_{\mathrm{E}}^{(n)}$. If the substructures are obtained through a partitioning of the FE mesh of the global structure, they are automatically conforming, as in Fig. 2(*a*), for which kinematic interface compatibility conditions require that

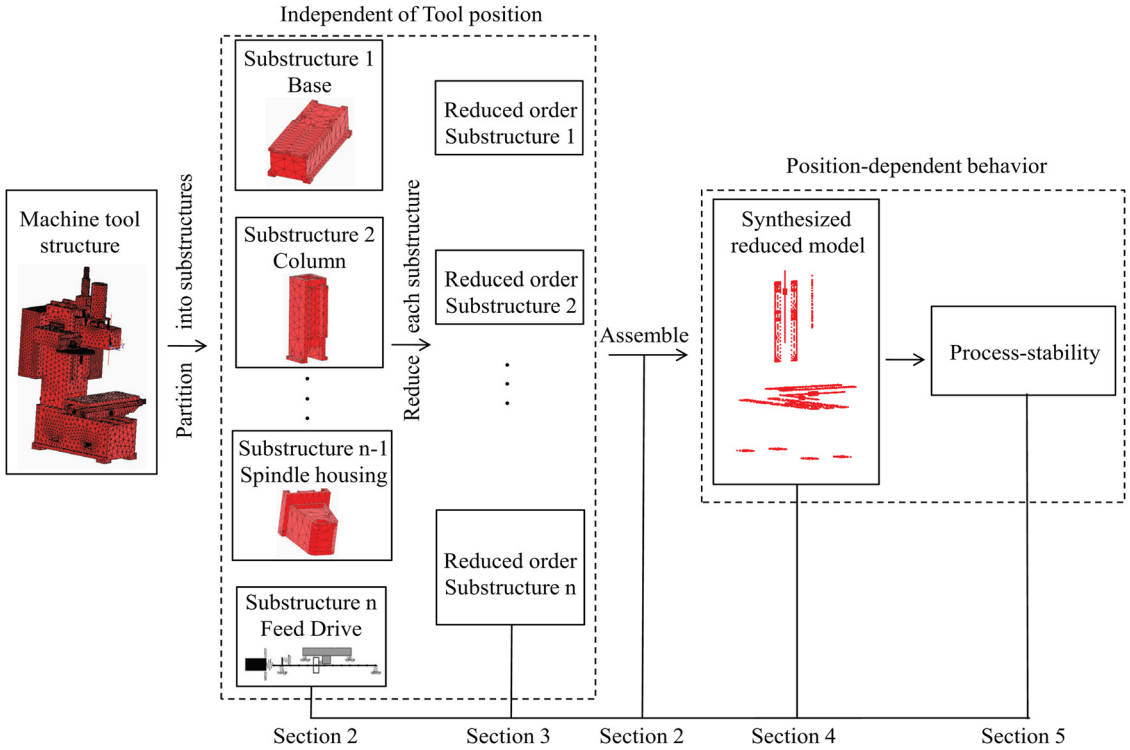

Fig. 1 Overview of the proposed modeling scheme

$$\boldsymbol{u}_{\mathrm{E}}^{(1)'} - \boldsymbol{u}_{\mathrm{E}}^{(2)'} = 0 \tag{1}$$

where $\boldsymbol{u}_{\mathrm{E}}^{(n)'}$ represents a subset of the total DOFs $\boldsymbol{u}_{\mathrm{E}}^{(n)}$ that are in contact at a particular position. The compatibility condition that extracts the interface DOFs is described by a displacement operator $\boldsymbol{C}^{(n)}$ of the form of a Boolean matrix represented as

$$\boldsymbol{C}^{(n)}\boldsymbol{u}^{(n)} = \begin{bmatrix} \boldsymbol{I}_{\mathrm{E}}^{(n)'} & 0 & 0 \end{bmatrix} \begin{Bmatrix} \boldsymbol{u}_{\mathrm{E}}^{(n)'} \\ \boldsymbol{u}_{\mathrm{E}}^{(n)} - \boldsymbol{u}_{\mathrm{E}}^{(n)'} \\ \boldsymbol{u}_{\mathrm{I}}^{(n)} \end{Bmatrix} \tag{2}$$

If however, the substructures are modeled separately with different mesh resolutions at interfaces, or by using dissimilar element types, as in Fig. 2(*b*), the displacement operator $\boldsymbol{C}^{(n)}$ will no longer have the form of a Boolean matrix, and in order to enforce approximate geometric compatibility between substructures, Lagrange multipliers are generally introduced [16]. The Lagrange multipliers approximated by shape functions are not suitable for a position-dependent formulation, since, each time one substructure moves over another (say, by changing Δr—Fig. 2), a different set of nodes come into contact at the interface, and employing the method in Ref. [16] would require a new set of Lagrange multipliers for each new position.

To synthesize such substructures with incompatible meshes, an approximate model of surface interaction is obtained by defining a virtual condensation node placed at the center of each of the interface surfaces in contact, as shown in Fig. 2(*b*), and subsequently enforcing displacement compatibility between these virtual nodes as

$$\boldsymbol{u}_{\mathrm{C}}^{(1)} - \boldsymbol{u}_{\mathrm{C}}^{(2)} = 0 \tag{3}$$

The displacement of the virtual node $\boldsymbol{u}_{\mathrm{C}}^{(n)}$ consisting of a set of translational and rotational DOFs ($\boldsymbol{u}_C \supset x_C, y_C, z_C, \theta_{xC}, \theta_{yC}, \theta_{zC}$) is linked to the interface DOFs with a displacement operator such that

$$\boldsymbol{u}_{\mathrm{C}}^{(n)} = \boldsymbol{C}^{(n)}\boldsymbol{u}^{(n)} \tag{4}$$

Coefficients of the displacement operator $\boldsymbol{C}^{(n)}$ are extracted by linking the DOFs of the condensation node to the interface nodal DOFs it is meant to represent ($\boldsymbol{u}_{\mathrm{E}}^{(n)'}$) using a multipoint constraint (MPC) equation formulation. The MPCs represent the DOFs of the condensation node as a linear combination of all the DOFs of the nodes in contact at the interface.

2.2 Multipoint Constraint Equation Formulation. Flexible bodies can be loaded in a multitude of nodal DOFs simultaneously, making force interactions possible over the entire contacting interface. To avoid the issue of multiple solutions made possible by the condensation node representing only a subset of these simultaneously loaded DOFs, all interface nodal DOFs are represented by the condensation node DOFs using constraint equations without any interface reduction. The condensation node hence describes a net translational and rotational motion of the nodes of the interface surface it represents.

All interface DOFs in contact are linked to the DOFs of the condensation node with the rigid MPC and the interpolation MPC [17].The formulation presented here, is for the generalized case of an individual substructural interface, hence the substructure superscript n is dropped.

2.2.1 Rigid Multipoint Constraints. A rigid MPC formulation links the DOFs in contact such that part of the interface surface in contact and the condensation node move as a rigid system. For each interface node k being linked to the condensation node, the displacement $\boldsymbol{u}_{\mathrm{E}_k'}$ is fully defined by the displacement $\boldsymbol{u}_C$ and the orientation $\boldsymbol{\alpha}_C$ of the condensation node as Ref. [17]

$$\boldsymbol{u}_{\mathrm{E}_k'} = \boldsymbol{u}_C + \boldsymbol{\alpha}_C \times \boldsymbol{r}_{Ck} \tag{5}$$

where $\boldsymbol{r}_{Ck}$ is the vector from the condensation node to the node corresponding to the interface node k. The orientation of the node is represented by rotations around linear coordinate axes by assuming small angle approximations. The set of nodal DOFs for each node k for volumetric elements in this work is represented as: $\boldsymbol{u} \supset x_k, y_k, z_k$. The rigid MPC formulation introduces as many constraints as the interface DOFs it represents, less the DOFs of the condensation node.

2.2.2 Interpolation Multipoint Constraints. The interpolation MPC formulation defines displacements and rotations of the condensation node as the weighted average of the motion of the interface nodes in contact. The motion of the condensation node is fully described by the displacement of all interface nodes in contact for a total of p exterior DOFs as Ref. [17]

$$\begin{aligned} \boldsymbol{u}_C &= \frac{\sum_{k=1}^{p} w_{\mathrm{E}_k} \boldsymbol{u}'_{\mathrm{E}_k}}{\sum_{k=1}^{p} w_{E_k}} \\ \boldsymbol{\alpha}_C &= \frac{\sum_{k=1}^{p} w_{\mathrm{E}_k} \boldsymbol{r}_{Ck} \times \boldsymbol{u}'_{\mathrm{E}_k}}{\sum_{k=1}^{p} w_{\mathrm{E}_k} |\boldsymbol{r}_{Ck}|^2} \end{aligned} \tag{6}$$

where w_{E_k} represents the weight factors for each DOF. An interpolation MPC formulation introduces as many additional constraints as there are condensation DOFs.

To ensure that the condensation node represents the average motion of the contacting interface, the weight factors w_{E_k} for each DOF are chosen proportional to the part of the interface surface its node represents; and are assigned as the coordinates of the nodes being coupled in this study. Since the modeling scheme is deliberately flexible to incorporate different substructures modeled using different mesh resolutions, the weights of all DOFs for an irregular mesh may not equal and may result in some DOFs being more heavily weighted than others.

2.3 Numerical Methods to Handle Constraint Equations. On account of constraining the displacements at the interface, there is an increase in the potential energy of the system. The potential function is modified by adding an extra "energy" term and is solved by the penalty method; and, the Lagrange multiplier method.

2.3.1 Penalty Method. The variation of the modified potential functional in its standard form yields [18]

$$\left[\boldsymbol{K} + \boldsymbol{C}^T \boldsymbol{\alpha} \boldsymbol{C}\right] \boldsymbol{u} = \boldsymbol{f} \tag{7}$$

where $\boldsymbol{C}$ is the displacement operator whose coefficients are extracted from Eq. (5) or (6); $\boldsymbol{C}^T\boldsymbol{\alpha}C$ is the penalty matrix, $\boldsymbol{\alpha} = \mathrm{diag}[\,\alpha_1 \quad \alpha_2, \ldots, \quad \alpha_m\,]$ is a diagonal matrix of m penalty numbers corresponding to the m constraint equations, $\boldsymbol{K}$ is the stiffness matrix, and $\boldsymbol{f}$ is the external force vector. If $\boldsymbol{\alpha} = 0$ in Eq. (7), the system of equations returns to the case of no constraints being imposed. As α_i ($i = 1,\ldots,m$) becomes very large, the penalty of violating constraints becomes large, so the constraints are closely satisfied. Numerical stability of this method is a function of the choice of α_i, which are selected based on guidelines as described in Ref. [18].

2.3.2 Lagrange Multiplier Method. By using a discrete set of m Lagrange multipliers ($\boldsymbol{\lambda}$) corresponding to m constraint equations, the form of the modified potential functional after the first variation is Ref. [18]

$$\begin{bmatrix} \boldsymbol{K} & \boldsymbol{C}^T \\ \boldsymbol{C} & 0 \end{bmatrix} \begin{Bmatrix} \boldsymbol{u} \\ \boldsymbol{\lambda} \end{Bmatrix} = \begin{Bmatrix} \boldsymbol{f} \\ 0 \end{Bmatrix} \tag{8}$$

As opposed to the penalty methods, the constraints are always satisfied in the Lagrange multiplier method. However, the size of the stiffness matrix increases by the factor of the number of Lagrange multipliers employed.

2.4 Substructural Synthesis. The assembled undamped equation of motion ensuring compatibility at the interfaces for the two substructures in Fig. 2 is represented as

$$\begin{bmatrix} \boldsymbol{M}^{(1)} & 0 \\ 0 & \boldsymbol{M}^{(2)} \end{bmatrix} \begin{Bmatrix} \ddot{\boldsymbol{u}}^{(1)} \\ \ddot{\boldsymbol{u}}^{(2)} \end{Bmatrix} + \begin{bmatrix} \boldsymbol{K}^{(1)} + \boldsymbol{C}^T \boldsymbol{\alpha} \boldsymbol{C} & 0 \\ 0 & \boldsymbol{K}^{(2)} + \boldsymbol{C}^T \boldsymbol{\alpha} \boldsymbol{C} \end{bmatrix} \begin{Bmatrix} \boldsymbol{u}^{(1)} \\ \boldsymbol{u}^{(2)} \end{Bmatrix} = \begin{Bmatrix} \boldsymbol{f}^{(1)} \\ \boldsymbol{f}^{(2)} \end{Bmatrix} \tag{9}$$

for the penalty method, and

$$\begin{bmatrix} \boldsymbol{M}^{(1)} & 0 & 0 \\ 0 & \boldsymbol{M}^{(2)} & 0 \\ 0 & 0 & 0 \end{bmatrix} \begin{Bmatrix} \ddot{\boldsymbol{u}}^{(1)} \\ \ddot{\boldsymbol{u}}^{(2)} \\ \ddot{\lambda}^{(12)} \end{Bmatrix} + \begin{bmatrix} \boldsymbol{K}^{(1)} & 0 & \boldsymbol{C}^T \\ 0 & \boldsymbol{K}^{(2)} & \boldsymbol{C}^T \\ \boldsymbol{C} & \boldsymbol{C} & 0 \end{bmatrix} \begin{Bmatrix} \boldsymbol{u}^{(1)} \\ \boldsymbol{u}^{(2)} \\ \boldsymbol{\lambda}^{(12)} \end{Bmatrix} = \begin{Bmatrix} \boldsymbol{f}^{(1)} \\ \boldsymbol{f}^{(2)} \\ 0 \end{Bmatrix} \tag{10}$$

for the Lagrange multiplier method; where $\{\boldsymbol{M}, \boldsymbol{K}\}$ are the substructural mass and stiffness matrices; and $\boldsymbol{C}(\boldsymbol{u}^{(1)}, \boldsymbol{u}^{(2)})$ is the displacement operator coupling the substructures. Employing the floating frame of reference technique, these sets of equations, i.e., the eigenvalue problem form of Eqs. (9) and (10), is solved for any desired position, by varying the position of the substructure 2, set by Δr (Fig. 2); thus obtaining the dynamic response at any position. The proposed formulation presents a complete description of modeling the position-dependent dynamics based on defining constraint equations to synthesize substructures.

3 Model Order Reduction

The substructural assembly formulation in Eqs. (9) and (10) may be treated as a generic CMS [16,19]. Consider the equation of motion for the case of undamped FE substructures:

$$\boldsymbol{M}\ddot{\boldsymbol{u}} + \boldsymbol{K}\boldsymbol{u} = \boldsymbol{f} \tag{11}$$

where $\{\boldsymbol{M}, \boldsymbol{K}\} \in Q^{f \times f}$ and $\boldsymbol{f} \in Q^{f \times 1}$. The general concept of model order reduction in structural mechanics is to find a low order subspace $\boldsymbol{T} \in Q^{f \times q}, q \ll f$, to approximate the displacement vector in Eq. (2) such that:

$$\boldsymbol{u}_{f \times 1} = \boldsymbol{T}_{f \times q} \boldsymbol{u}_{\boldsymbol{r}_{q \times 1}} \tag{12}$$

where $\boldsymbol{T}$ is the transformation matrix for reduction and $\boldsymbol{u}_{\boldsymbol{r}}$ is the reduced displacement vector.

The reduced structural matrices by way of projection on the subspace $\boldsymbol{T}$ become

$$\boldsymbol{M}_{R_{q \times q}} = \boldsymbol{T}^T \boldsymbol{M} \boldsymbol{T}; \quad \boldsymbol{K}_{R_{q \times q}} = \boldsymbol{T}^T \boldsymbol{K} \boldsymbol{T}; \quad \boldsymbol{f}_{R_{q \times 1}} = \boldsymbol{T}^T \boldsymbol{f} \tag{13}$$

Since the reduction procedure involves eliminating a subset of DOFs from $\boldsymbol{u}$, the system matrices are partitioned into exterior/interface DOFs (E), and interior DOFs (I) as

$$\begin{bmatrix} \boldsymbol{M}_{EE} & \boldsymbol{M}_{EI} \\ \boldsymbol{M}_{IE} & \boldsymbol{M}_{II} \end{bmatrix} \begin{Bmatrix} \ddot{\boldsymbol{u}}_E \\ \ddot{\boldsymbol{u}}_I \end{Bmatrix} + \begin{bmatrix} \boldsymbol{K}_{EE} & \boldsymbol{K}_{EI} \\ \boldsymbol{K}_{IE} & \boldsymbol{K}_{II} \end{bmatrix} \begin{Bmatrix} \boldsymbol{u}_E \\ \boldsymbol{u}_I \end{Bmatrix} = \begin{Bmatrix} \boldsymbol{f}_E \\ \boldsymbol{f}_I \end{Bmatrix} \tag{14}$$

The transformation matrix for the standard CMS-Craig and Bampton method, which contains the entire set of constraint modes and a set of component normal modes is [19]

$$\boldsymbol{T}_{\text{CMS}} = \begin{bmatrix} \boldsymbol{I}_{EE} & 0_{EP} \\ \boldsymbol{T}_{S_{IE}} & \boldsymbol{\Phi}_{IP} \end{bmatrix} \tag{15}$$

where $\boldsymbol{I} \in Q^{E \times E}$ is a unit matrix; and $\boldsymbol{T}_{S_{IE}} = -\boldsymbol{K}_{II}^{-1} \boldsymbol{K}_{IE}$ is the equivalent static (Guyan) transformation [20].

$\boldsymbol{\Phi}_{IP} \subseteq \boldsymbol{\Phi}_{II}$ in Eq. (15) is obtained by traditionally retaining the first few P modes of the mode shape vector $\boldsymbol{\Phi}_{II}$; which is obtained by solving the eigenvalue problem corresponding to the interior DOFs of the form

$$\left[\boldsymbol{K}_{II} - \omega^2 \boldsymbol{M}_{II}\right] \boldsymbol{\Phi}_{II} = 0 \tag{16}$$

To overcome the quasi-static nature of the transformation in Eq. (15), advantageous characteristics of another model order reduction scheme, the so-called iterated "improved reduction system" (IRSi) method based on Refs. [21–23] are included. The new iterated improved component mode synthesis transformation matrix becomes [23]

$$\boldsymbol{T}_{\text{ICMS}_{i+1}} = \begin{bmatrix} \boldsymbol{I}_{EE} & 0_{EP} \\ \boldsymbol{T}_{IRS_{i+1_{IE}}} & \boldsymbol{\Phi}_{IP} \end{bmatrix} \tag{17}$$

The iterated IRS terms are [23]

$$\boldsymbol{T}_{\text{IRS}_{i+1}} = -\boldsymbol{K}_{II}^{-1} \boldsymbol{K}_{IE} + \boldsymbol{K}_{II}^{-1} \left(\boldsymbol{M}_{IE} + \boldsymbol{M}_{II} \boldsymbol{T}_{ICMS,i}\right) \boldsymbol{M}_{\text{IRS,i}}^{-1} \boldsymbol{K}_{\text{IRS,i}} \tag{18}$$

where $\boldsymbol{T}_{\text{ICMS}} = \begin{bmatrix} \boldsymbol{I}_{EE} & 0_{EP} \\ \boldsymbol{T}_{\text{IRS}_{IE}} & \boldsymbol{\Phi}_{IP} \end{bmatrix}$, where in $\boldsymbol{T}_{\text{IRS}} = -\boldsymbol{K}_{II}^{-1} \boldsymbol{K}_{IE} + \boldsymbol{K}_{II}^{-1} \boldsymbol{S} \boldsymbol{M}_{R_S}^{-1} \boldsymbol{K}_{R_S}$; and, $\boldsymbol{S} = \boldsymbol{M}_{IE} - \boldsymbol{M}_{II} \boldsymbol{K}_{II}^{-1} \boldsymbol{K}_{IE}$. The reduced matrices, i.e., $\boldsymbol{M}_{R_S}; \boldsymbol{M}_{\text{IR}_S\text{,i}}; \boldsymbol{K}_{R_S}; \boldsymbol{K}_{\text{IR}_S\text{,i}}$ are obtained with appropriate projections onto reduced subspaces as in Eq. (13).

3.1 Mode Selection Criteria. To obtain position-independent substructural reduced models, the mode sets in Eq. (17), i.e., P modes of the mode shape vector $\boldsymbol{\Phi}_{II}$, i.e., $\boldsymbol{\Phi}_{IP} \subseteq \boldsymbol{\Phi}_{II}$ are selected using the approach as detailed in the flowchart given in Fig. 3.

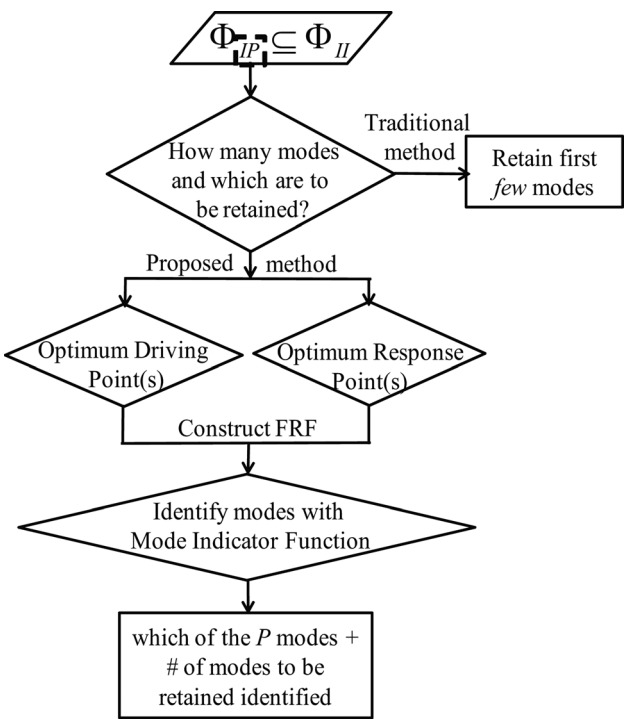

Fig. 3 Flow chart for determining mode cut-off number

In experimental modal analysis actuators are placed at locations to excite all the modes in the frequency range of interest, and, sensors are placed at locations where these modes achieve a high observability. Significant modes are treated as those identified with a mode indicator function from the measured FRF. A similar methodology is used in this work, except that the measured FRFs are replaced by simulated FRFs.

To determine the optimal excitation location, the "optimum driving point(s) (ODP)" method [24] is employed since it offers a very 'natural' selection criterion based on the computed eigenvectors ($\mathbf{\Phi}_{II}$). Point(s) with large mode shape amplitudes for the modes of interest are selected while avoiding the nodal points or any points near the nodal line. The ODP parameter for a DOF, v, is defined as [24]

$$\mathrm{ODP}_v = \prod_{r=1}^{l} \|\Phi_{II_{v_r}}\| \tag{19}$$

where l is the number of modes of interest. The DOF that has the largest ODP parameter is considered as the possible excitation location.

To determine the response location, the point with the maximum kinetic energy is chosen. The energy distribution method is employed here, as it involves computing the kinetic energy, which is a direct measure of the structural properties. The kinetic energy (KE) at the uth DOF for l modes of interest is [25]

$$KE_u = \frac{\mathbf{M}_{II_{uu}}}{2} \sum_{r=1}^{l} \omega_r^2 \Phi_{II_{u_r}}^2 \tag{20}$$

where ω_r is the undamped eigenfrequency obtained by solving the eigenvalue problem in Eq. (16); and $\mathbf{M}_{II}$ are the inertial terms corresponding to the interior DOFs obtained from Eq. (14).

A FRF ($\boldsymbol{H}_{uv}$) is simulated up to the frequency range of interest as

$$\boldsymbol{H}_{uv} = \sum_{r=1}^{l} \frac{\Phi_{II_{u_r}} \Phi_{II_{v_r}}}{-\omega^2 + i2\zeta\omega\omega_r + \omega_r^2} \tag{21}$$

where $\Phi_{II_{u_r}}$ is the eigenvector at the optimal response location DOF u; $\Phi_{II_{v_r}}$ is the eigenvector at the optimal driving point DOF v; ζ is the damping ratio; ω_r is the natural frequency; and i is the imaginary operator. To identify the number of modes in this FRF, which are to be treated as significant, a mode indicator hunction (MIF) is employed which is defined at each frequency point, s, for a total of N points as [24]

$$\mathrm{MIF}(s) = \frac{\sum_{s=1}^{N} |Re(H_{uv})||H_{uv}|}{\sum_{s=1}^{N} \lfloor H_{uv}^2 \rfloor} \tag{22}$$

The equations of motion in Eqs. (9) and (10), are modified with the transformation of Eq. (17) complemented with proper sorting and selection of the component modes to be retained as described above; to yield substructurally sysnthesied reduced order models.

4 Application: Modeling a Three Axis Milling Machine

The position-dependency of the dynamic stiffness at the TCP of a machine tool is primarily due to the relative motion of the spindle-spindle housing moving over the vertical column. Hence, as a first step, only the spindle, spindle housing, and column substructures are modeled, reduced independently, and combined subsequently using constraint formulations. The spindle assembly including the tool-tool-holder, spindle shaft, spindle cartridge, bearings, spacers, drive pulley, and other accessories such as nuts and rotary couplings is integrated as a separate substructure coupled rigidly to the spindle housing. The spindle shaft, spindle cartridge, and the tool-tool-holder combination are all modeled with Timoshenko beam elements. Bearings are modeled as radial-axial springs, and other accessories are modeled as lumped mass elements as described in Ref. [26]. The tool-tool-holder-spindle interface connections are assumed to be rigid. FE models for structural substructures have been generated from their respective detailed CAD models using ten noded solid tetrahedron elements. The structural components were assigned material properties as: modulus of Elasticity of 89 GPa; density of 7250 kg/m^3; and, Poisson's ratio of 0.25. The assembled model is assumed to be rigidly connected to the machine base. All other structural elements (base, cross-slide, etc.), and machine accessories are ignored. After necessary convergence tests of FE models, the substructural system matrices were exported to the MATLAB environment. All subsequent model order reduction and model synthesis were conducted within the MATLAB environment.

4.1 Model Order Reduction for Substructures. The reduced substructural model consist of interface DOFs complemented by a set of component generalized coordinates, as listed in Table 1. The interface DOFs for the column substructure represent the guide-way top surfaces and surfaces in contact with the machine base; and, for the spindle-spindle housing substructure the interface DOFs represent the guide-block surfaces in contact with the guide-ways and the DOFs corresponding to the spindle assembly including the tool-tool holder DOFs. The generalized coordinates correspond to the significant modes identified with the mode indicator function from the FRF simulated up to 10 kHz between the optimal driving and response locations. Uniform damping of the level of $\zeta = 0.02$ is assumed for all modes. In this way, 31 significant modes are identified for the spindle-spindle housing substructure, and 43 for the column substructure.

Table 2 compares the first 15 significant modes identified for the representative column substructure using the mode indicator function based sorting scheme with that of the standard CMS modal reduction scheme, i.e., in which the first few ($P = 15$) non-rigid-body low frequency modes are retained. As is evident in representative results in Table 2, the mode sets are disjoint; and, that the mode indicator function based ranking scheme spans a wider frequency range than the standard modal reduction. For the standard modal reduction scheme to span the same frequency range as that of the mode indicator function based scheme, 310 mode sets would need to be retained for the column substructure, instead of the 43 presently identified as significant. In the case of the spindle-spindle housing substructure, 139 modes would need to be retained instead of the 31 identified as significant. The reduced set hence includes effects of higher order dynamics while keeping the reduced size to a minimum while automatically deciding the order of the reduced model.

4.2 Verification of the New Improved Reduced Order Model. To determine the accuracy of the improved reduced order model over the standard CMS scheme; and to validate them; two criteria are employed: the normalized relative frequency

Table 1 Division of DOFs for the substructural components

		Column	Spindle-spindle housing	Total
Full order model		10908	15117	26025
Reduced Model	Interface DOFs ($\boldsymbol{u}_E$)	762	1845	2681
	Significant component modes (P)	43	31	

Table 2 Top 15 mode subsets for standard CMS modal reduction (SMR) and MIF based sorting for the column substructure

SMR	Mode #	1	2	3	4	5	6	7	8	9	10	11	12	13	14	15
	Freq. $\times 10^3$ (Hz)	0.21	0.48	0.6	0.68	0.87	0.92	0.93	0.96	1.02	1.14	1.17	1.21	1.33	1.37	1.39
MIF	Mode #	1	4	5	7	9	11	12	13	14	16	22	25	27	28	32
	Freq. $\times 10^3$ (Hz)	0.21	0.68	0.87	0.93	1.02	1.17	1.21	1.33	1.37	1.47	1.64	1.74	1.83	1.89	2.07

difference; and, the modal assurance criterion. The normalized relative frequency difference (NRFD) is defined as

$$\mathrm{NRFD}_{(r)} = \left|1 - \frac{f_{\mathrm{full}}}{f_{\mathrm{ROM}}}\right|.100\%, \quad r = 1, 2, \ldots, l \tag{23}$$

where f_{full} and f_{ROM} are the eigenfrequencies of the full order model and the reduced order model, respectively. The modal assurance criterion (MAC) in turn is defined as [24]

$$\mathrm{MAC} = \frac{\left|\boldsymbol{\Phi}_{\mathrm{full}}^{\mathrm{T}}\boldsymbol{\Phi}_{\mathrm{ROM}}\right|^2}{\left(\boldsymbol{\Phi}_{\mathrm{full}}^{\mathrm{T}}\boldsymbol{\Phi}_{\mathrm{full}}\right)\left(\boldsymbol{\Phi}_{\mathrm{ROM}}^{\mathrm{T}}\boldsymbol{\Phi}_{\mathrm{ROM}}\right)} \tag{24}$$

where $\boldsymbol{\Phi}_{\mathrm{full}}$ and $\boldsymbol{\Phi}_{\mathrm{ROM}}$ are the mode shape vectors for the full and the reduced order model, respectively. Generally, MAC values in excess of 0.9 should be attained for well-correlated modes and a value of less than 0.1 for uncorrelated modes.

All substructures were verified, though only results for the column are reported. The column substructure has less interface DOFs than the spindle-spindle housing substructure, making it more stringent with to have proved verification. Figure 4 compares the NRFD and MAC of the first 80 modes, for the column substructure; between the standard Craig–Bampton CMS method including standard modal reduction based sorting scheme, and that of the iterated improved component mode synthesis with mode indicator based sorting scheme. The improved reduced order model has a frequency error of less than 1% for entire frequency spectrum considered, while the standard CMS method has errors as high as 60% for the high frequency modes. Similarly, the improved reduced order model is far better correlated to the full order model than the standard CMS scheme, having diagonal dominated near uniform unity MAC values; hence, making it the method employed for all subsequent analysis.

4.3 Substructural Assembly for Different Positions of Substructures. Consider the case of the spindle-spindle housing combination in rigid contact with the column as shown in Fig. 5. Each of the four pairs of contacting interfaces between the four spindle-housing guide-block sets and the column guide-ways is represented by a pair of condensation nodes linked to the interface DOFs using multipoint constraint formulations of Eqs. (5) and (6). The weight factors w_{E_k} in Eq. (6) are assigned as the nodal coordinates. The modified (reduced) form of the synthesized constrained equation sets of Eqs. (9) and (10) are solved using the penalty method from Eq. (7) as well as the Lagrange multiplier method from Eq. (8). To evaluate the reduced order substructurally synthesized position-dependent model, TCP FRFs simulated assuming uniform damping of the level of $\zeta = 0.02$ for all modes are compared with that of a full order model obtained from ANSYS [27], wherein the substructures were 'glued' together.

To evaluate the effect of the type of constraint formulation, results with different MPC formulations are compared in Fig. 6 (top). The rigid MPC formulation overestimates stiffness, which in turn results in higher eigenfrequency estimates. The FRF for the rigid MPC seems to have shifted to right when compared with the full order model FRF, while the FRF with the interpolation MPC formulation reasonably approximates full order response, and hence is recommended as the method of choice to be employed for subsequent synthesis. Furthermore, results with different numerical solution schemes to the constrained problem, i.e., with the Lagrange multiplier method and the penalty method

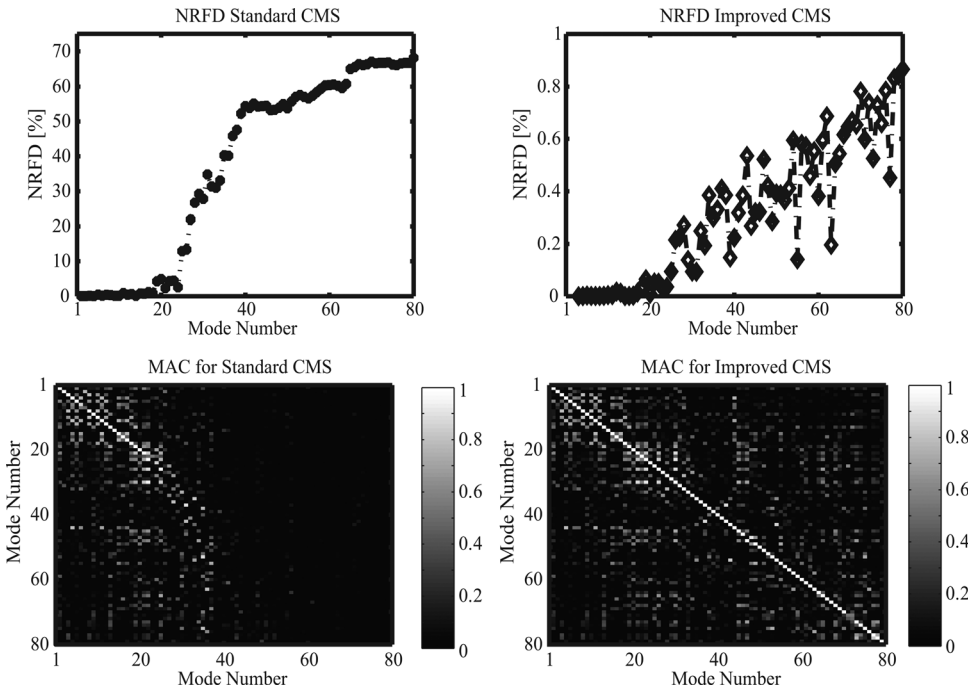

Fig. 4 NRFD and MAC comparison for standard component mode synthesis scheme (left) and iterated improved component mode synthesis scheme (right)

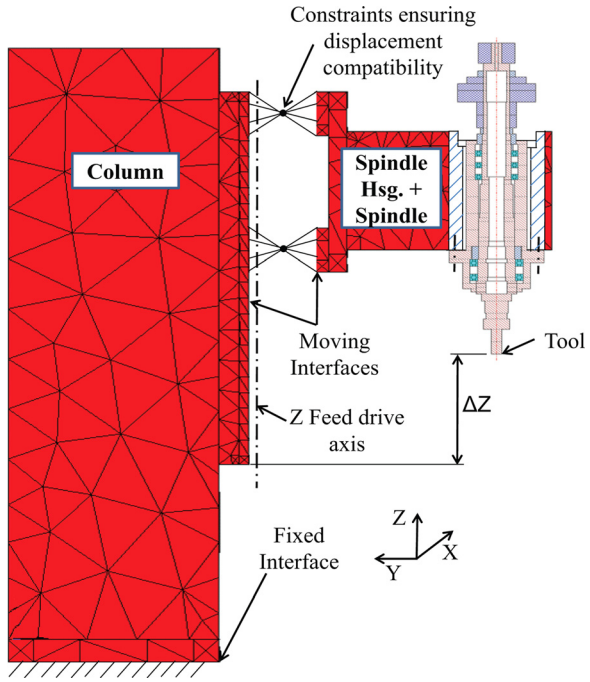

Fig. 5 Substructural assembly of the spindle-spindle housing substructure with the column substructure through constraint formulations

are also compared in Fig. 6 (bottom). For penalty numbers selected as $\alpha_{i\forall m} = 1 \times 10^5 \times \max(\mathrm{diag}[\boldsymbol{K}])$ [18] both methods give the same response.

As a second step, position-dependent response comparisons between the substructurally synthesized reduced order models and full order models are shown in Fig. 7. The substructural synthesis

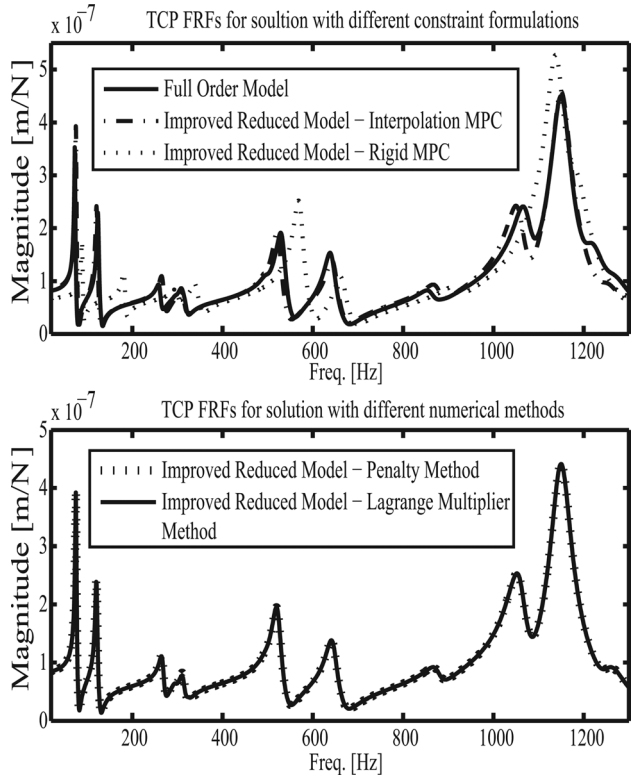

Fig. 6 Comparison of TCP FRFs for solution: with different constraint formulations (top), and with different numerical methods (bottom)

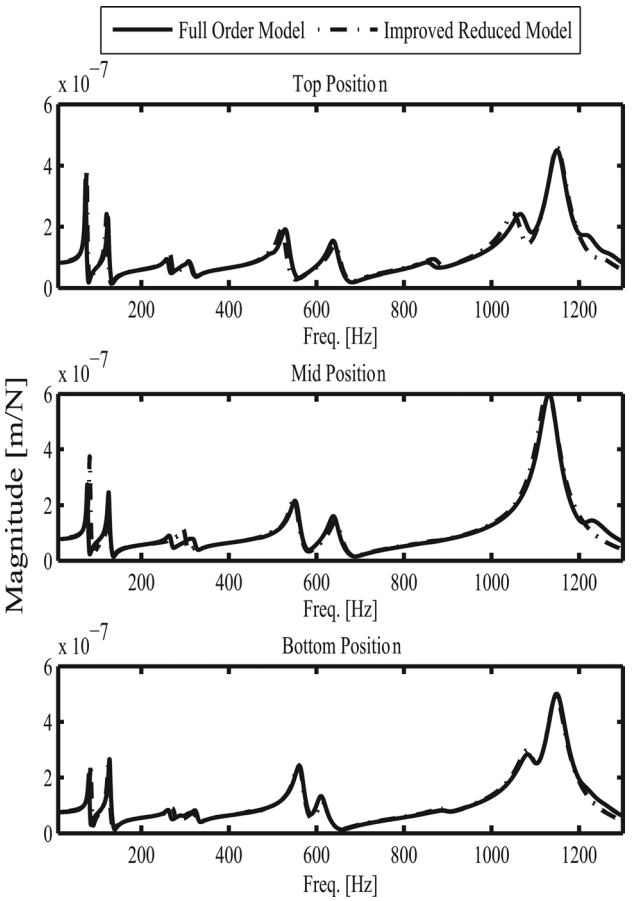

Fig. 7 Comparison of full order model and reduced order model TCP FRFs at three different positions: top position (top), mid position (middle), and bottom position (bottom)

being based on a floating frame of reference system, the moving frame attached to the TCP is adjusted relative to the reference frame by varying ΔZ (in Fig. 5). For each new position, a new set of constraint equations are established to describe the relations between the new nodes that have come into contact, by suitably updating the displacement operator, $\boldsymbol{C}$, within Eq. (9) or (10). Subsequently, the new reduced synthesized constrained equation sets of Eq. (9) or (10) are solved to obtain the position-dependent response. Three different positions are compared: the configuration when the spindle-spindle housing is at the top position, as shown in Fig. 5; a mid position; and, a bottom position when the spindle-spindle housing combine has moved in the Z-direction by an amount of −0.2 m; and −0.4 m, respectively.

In addition, Table 3 compares the natural frequencies and dynamic stiffness at the different positions. As is evident, the global modes corresponding to the column (up to 150 Hz) and the spindle housing (up to 600 Hz) exhibit strong position-dependent behavior, varying by 6–10% in natural frequencies and by 50–75% in dynamic stiffnesses. The spindle-tool-tool-holder modes (600–1200 Hz) on the other hand are more local in nature and do not exhibit strong position-dependency.

The synthesized reduced model is able to reasonably approximate full model behavior and being ∼1/10th the size of the full model (see Table 1) leads to considerable simulation time savings; taking ∼10 s/position as compared to ∼6 h/position for the 'full' model (Intel® i3-380 M processor with 4 GB RAM) thereby facilitating further position-dependent stability analysis.

5 Position-Dependent Stability

During machining, the frequency content of the force signal may excite one or more of the structural modes of the machine

Table 3 Comparison of position-dependent behavior for the improved reduced model

Mode #	Top position Freq. (Hz)	Top position Dynamic stiffness (N/μm)	Mid position Freq. (Hz)	Mid position Dynamic stiffness (N/μm)	Bottom position Freq. (Hz)	Bottom position Dynamic stiffness (N/μm)	Associated mode shape
1	73	2.8	77	3.7	81	4.8	Global column bending
2	124	4.4	125	4.1	128	3.8	Global spindle-housing + column bending
3	258	10.7	263	11.1	260	12.2	Global spindle-housing bending
4	310	11.6	318	12.6	325	12.5	Global spindle-housing bending + torsion
5	529	5.2	550	4.6	561	4.1	Global spindle-housing torsion
6	639	6.5	640	6.2	612	7.6	Spindle bending
7	853	12.1	—	—	889	12.2	Spindle + tool-tool holder bending
8	1066	4.1	—	—	1083	3.6	Tool-tool holder bending
9	1149	2.1	1131	1.7	1148	2	Tool-tool holder bending

Table 4 Cutting parameters used in process-stability simulations

	Case 1	Case 2
Type of Cutter	20 mm diameter solid end mill, 30 deg helix	20 mm diameter solid end mill, 30 deg helix
Number of teeth on cutter, N_t	4	4
Overhang from spindle nose	220 mm	220 mm
Workpiece material	AISI 1045 Steel	Al 7075-T6
Tangential cutting coefficient, K_t	1904 MPa	796 MPa
Radial cutting constant, K_r	0.62	0.212
Immersion	Full (100%)	Full (100%)

tool. This excitation may lead to a regenerative chatter mechanism, which is strongly influenced by the modal parameters of the machine tool. Moreover, because the machine model can now be efficiently reconfigured and assembled in any desired position, this model may be utilized in characterizing the effects of process machine interactions by way of predicting the position-dependent stability.

The position-dependent chatter stability of the milling system is determined using a modal model of the machine and the following characteristic equation [28]:

$$\det([\boldsymbol{I}] - \Lambda[\boldsymbol{\alpha}_0][\boldsymbol{\Phi}(i\omega_c)]) = 0 \tag{25}$$

where

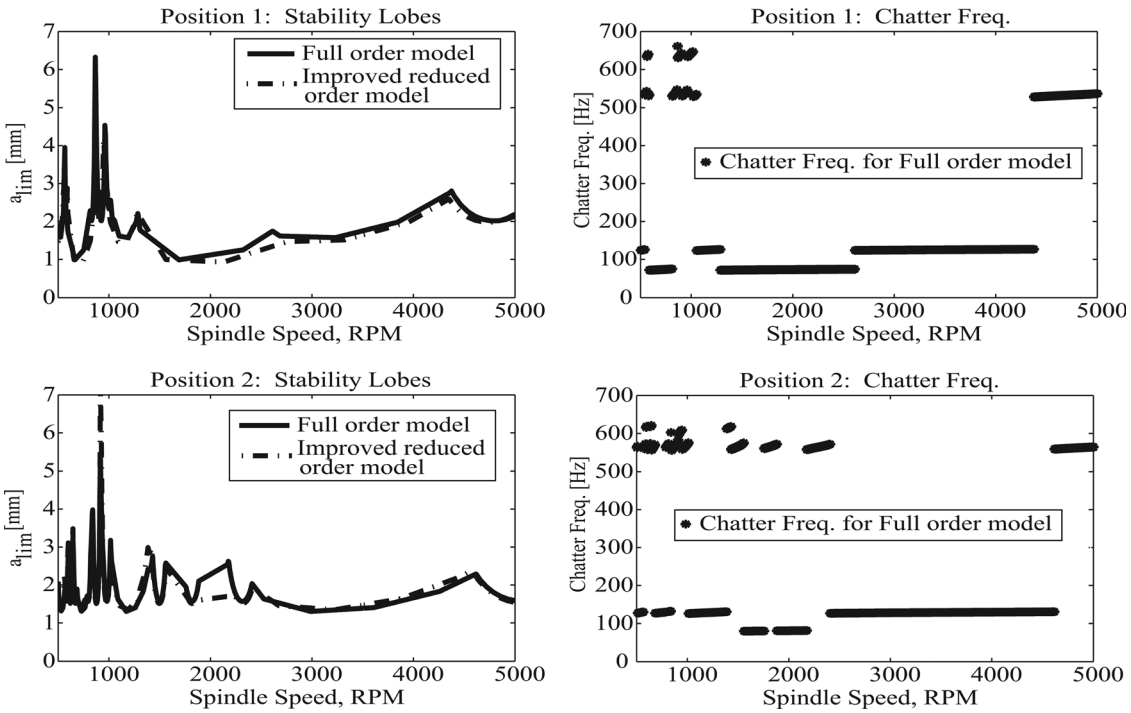

Fig. 8 Stability boundaries at two distinct positions (left) and the corresponding chatter frequencies (right) for machining AISI 1045 common steel

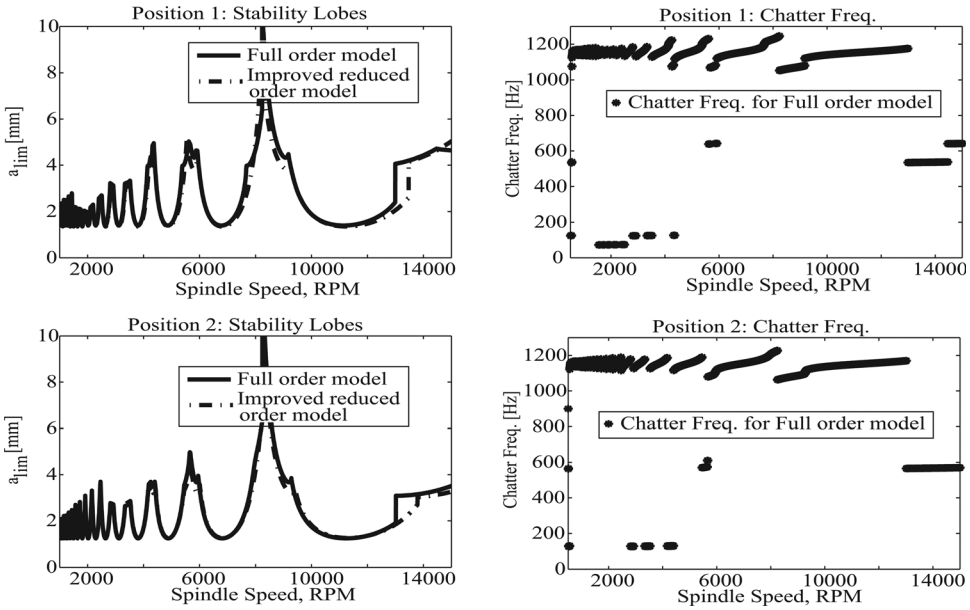

Fig. 9 Stability boundaries at two distinct positions (left) and the corresponding chatter frequencies (right) for machining Al 7075-T6

$$\Lambda = \Lambda_R + i\Lambda_I = -\frac{1}{4\pi} N_t K_t a\left(1 - e^{-i\omega_c T}\right) \tag{26}$$

is the eigenvalue of the characteristic equation; Λ_R and Λ_I are its real and imaginary parts; N_t is the number of teeth on the cutter; K_t is the cutting force coefficient of the material being cut; a is the axial depth of cut; ω_c is the chatter frequency; and, T is the tooth passing period.

In Eq. (25) $\boldsymbol{\alpha}_0$ is the matrix of the average direction factors, determined as in Ref. [28]; and $\boldsymbol{\Phi}$ is the position-dependent transfer function matrix at the TCP, represented as:

$$[\boldsymbol{\Phi}(i\omega)] = \begin{bmatrix} \Phi_{xx}(i\omega) & \Phi_{xy}(i\omega) \\ \Phi_{yx}(i\omega) & \Phi_{yy}(i\omega) \end{bmatrix} \tag{27}$$

where Φ_{xx} $(i\omega)$ and Φ_{yy} $(i\omega)$ are the direct transfer functions in the x and y directions, and Φ_{xy} $(i\omega)$ and Φ_{yx} $(i\omega)$ are the cross transfer functions. The mode directions are assumed to be orthogonal, hence the cross terms are negligible, i.e., $\Phi_{xy}(i\omega) = \Phi_{yx}(i\omega) = 0$ in the principal modal directions. To simulate the position dependent stability, $\boldsymbol{\Phi}$ $(i\omega)$ is updated for every position. The critically stable depth of cut ($a = a_{\text{lim}}$) is analytically determined as [28]

$$a_{\text{lim}} = -\frac{2\pi\Lambda_R}{N_t K_t}\left[1 + \left(\frac{\Lambda_I}{\Lambda_R}\right)^2\right] \tag{28}$$

Two examples have been presented, one for cutting steel and the other for cutting Al alloys to demostrate position-dependent process-machine interaction effects. Cutting conditions are as listed in Table 4. Simulated chatter stability lobes and the corresponding chatter frequencies are compared for the substructurally synthesized improved reduced order models with that of full order model results in Fig. 8 and 9; at two positions: position 1, i.e., top position and position 2, i.e., bottom position.

For the case of machining common steels such as AISI 1045 (Fig. 8), it is difficult to excite modes greater than 1000 Hz; the excitation frequency being limited by the recommend cutting speeds for milling of such materials [29]. Thence modes beyond this range are ignored in chatter simulation. Even though the TCP response is dominated by the high frequency spindle-tool-tool-holder modes, these mainly chatter at high speeds and are damped out by the cutting process in lower speed zone where the lower frequency column and spindle housing modes, which are position-dependent, chatter. As was evident in Fig. 7, for the low frequency range, the dynamic response at position 2 was stiffer than the response at position 1, which should manifest as the stability boundary for this position (position 2) being higher than that at position 1, which is the observed behavior in Fig. 8 (left). The strong shifts in chatter frequencies at spindle speeds of ~1500–2500 rpm, corresponding to the shifts in the global modes of the column and the spindle housing are also evident in Fig. 8 (right). The results with improved reduced order models are found to be in good agreement with the full order results, with the exception at spindle speed of ~2000 rpm for position 2; which may partially be attributed numerical errors.

If, however, the machine was envisaged to machine light Al alloys cut at high cutting (spindle) speeds, the local high-frequency spindle-tool-tool holder modes may also be excited. Including these modes in chatter simulation for machining such an alloy—Al 7075, i.e., for Case 2, a new set of stability lobes were obtained, as shown in Fig. 9 (left); along with the corresponding chatter frequencies Fig. 9 (right). For Case 2, the local tool-tool holder modes are dominant; as seen in Fig. 7. Hence, regardless of the position-dependent shift in the global structural modes, the stability boundaries overlap. The only significant position-dependent influence is observed in the high-speed range (~12,000–15,000 rpm) characterized by a lowering of the stability boundary in this region at position 2 corresponding to the shift in the global spindle housing modes (400–600 Hz); evident also in the shift in the chatter frequencies in Fig. 9 (right).

From Figs. 7–9 it may also be inferred that any local error in response estimation with the reduced models by under/over-estimation of particular modes translates to a local decrease/increase in the stability boundaries and the corresponding chatter frequencies.

6 Conclusions

A systematic and computationally efficient procedure is proposed to model and evaluate the position-dependent dynamic behavior of a three axis milling machine tool based on substructural synthesis of improved reduced order models as an alternative to presently used, time consuming full FE models by the

designers. Position-dependent dynamic stability was simulated on a representative three axis milling machine for two envisaged machining operations. It was demonstrated that the position-dependent response at the TCP as well as the machining operation impact the stability of the process.

Machine substructural components were reduced and subsequently synthesized using adaptations of constraint equations which tolerate mesh incompatibility at their contacting interfaces; allowing for modular design. Substructural components were reduced using an improved variant of the component mode synthesis method to retain interface DOFs complemented by a set of judiciously selected component modes using a novel mode selection criterion. The mode sets thus identified are able to represent higher order dynamics of the substructure while keeping the order of the reduced model to a minimum by spanning a much wider frequency range with fewer modes than would be required with standard CMS methods. Substructural syntheses with the interpolation MPC formulation were found to be better than the rigid MPC formulation. For a correct choice of the penalty number, both numerical solution techniques to the constrained problem provided the same results. Dynamic response characteristics of the substructurally synthesized reduced order FE models were verified against corresponding full order models.

The substructures were rigidly coupled in this study, without having modeled the stiffness and damping at the joints. Joint characteristics though severely affect tool point response, are difficult to model at the design stage and must be caliberated from measurements on similar already built machines, which is part of future research. The ultimate aim of this project is a complete co-simulation of the machine structural dynamics including the feed drive dynamics, the axis position control, the NC interpolation, and the process-machine interactions via a stability model. This synthesized mechatronic machine tool system will allow evaluation and optimization of the dynamic performance of the machine tool at the design stage, eliminating the need for costly physical prototyping.

Acknowledgment

This research has been supported by the NSERC CANRIMT Research Grant.

Nomenclature

a = axial depth of cut
a_{lim} = axial critically stable depth of cut
$\boldsymbol{C}$ = displacement operator
f = total number of degrees of freedom (DOF)
f_{full} = eigenfrequencies of the full order model
f_{ROM} = eigenfrequencies of the reduced order model
$\boldsymbol{f}$ = generalized force vector
$\boldsymbol{H}$ = frequency response function
i = imaginary operator
$\mathbf{I}$ = identity matrix
k = interface node
$\boldsymbol{K}$ = stiffness matrix
K_t = tangential cutting coefficient
K_r = radial cutting constant
l = number of modes of interest
m = number of constraint equations
$\boldsymbol{M}$ = mass matrix
n = substructure number
N = total number of frequency points
N_t = number of teeth
p = total number of exterior DOFs being represented by the condensation node
P = number of component modes retained
q = reduced order DOFs
Q = real space
r = counter for number of modes
$\boldsymbol{r}_{Ck}$ = vector from the condensation node to the node corresponding to the interface node k
s = number of frequency points
S = substructure
T = tooth passing period
$\boldsymbol{T}$ = transformation matrix
u = optimum response location
$\boldsymbol{u}$ = displacement vector
$\boldsymbol{u}_{\text{C}}$ = condensation node displacement vector
$\boldsymbol{u}_{\text{E}}$ = displacement vector corresponding to exterior DOFs
$\boldsymbol{u}_I$ = displacement vector corresponding to interior DOFs
$\boldsymbol{u}_r$ = reduced displacement vector
v = optimum driving point location
w_{E_k} = weight factor for DOF k
x, y, z = indicate parameters pertaining to the x, y, and z directions, respectively
$\theta_x, \theta_y, \theta_z$ = rotations about x, y, and z directions, respectively
α = penalty number
$\boldsymbol{\alpha}_C$ = orientation vector of the condensation node
$\boldsymbol{\alpha}_0$ = matrix of directional factors
ω = frequency
ω_c = chatter frequency
ω_r = eigenfrequency
$\boldsymbol{\lambda}$ = Lagrange multiplier
Λ = eigenvalues of the characteristic equation
Λ_R = real eigenvalues
Λ_I = imaginary eigenvalues
$\boldsymbol{\Phi}_{\text{full}}$ = mode shape vector for full order model
$\boldsymbol{\Phi}_{\text{ROM}}$ = mode shape vector for reduced order model
$\boldsymbol{\Phi}_{II}$ = eigenvector corresponding to the interior DOFs
$\boldsymbol{\Phi}\ (i\omega)$ = transfer function matrix
ζ = damping ratio
Δr = instantaneous position of substructure
ΔZ = instantaneous position of spindle-spindle housing substructure relative to the column
CMS = component mode synthesis
DOF = degree of freedom
FE = finite element
FRF = frequency response function
ICMS = improved CMS
$\text{ICMS}_{\text{i+1}}$ = iterated improved CMS
IRS = improved reduction system
$\text{IRS}_{\text{i+1}}$ = iterated improved reduction system
MAC = modal assurance criterion
MIF = mode indicator function
MPC = multipoint constraint
NRFD = normalized relative frequency difference
ODP = optimum driving point
TCP = tool center point
$\supset$ = includes, or is a superset of
$\in$ = is an element of
$\subseteq$ = subset of
Π = product over
$\|\ldots\|$ = norm of
$\forall$ = for each

References

[1] Altintas, Y., 2000, *Manufacturing Automation: Metal Cutting Mechanics, Machine Tool Vibrations, and CNC Design*, Cambridge University Press, New York.
[2] Sadek, M. M., and Tobias, S. A., 1970, "Comparative Dynamic Acceptance Tests for Machine Tools Applied to Horizontal Milling Machines," Proc. Inst. Mech. Eng., **185**, pp. 319–337.
[3] Bianchi, G., Paolucci, F., Van den Braembussche, P., Van Brussel, H., and Jovane, F., 1996, "Towards Virtual Engineering in Machine Tool Design," CIRP Ann., **45**, pp. 381–384.
[4] Zaeh, M. F., and Siedl, D., 2007, "A New Method for Simulation of Machining Performance by Integrating Finite Element and Multi-Body Simulation for Machine Tools," CIRP Ann., **56**, pp. 383–386.
[5] Aurich, J. C., Biermann, D., Blum, H., Brecher, C., Carstensen, C., Denkena, B., Klocke, F., Kroger, M., Steinmann, P., and Weinert, K., 2009, "Modelling and Simulation of Process: Machine Interaction in Grinding," Prod. Eng. Res. Dev., **3**, pp. 111–120.

[6] Okwudire, C., 2009, "Modeling and Control of High Speed Machine Tool Feed Drives," Ph.D. thesis, University of British Columbia, Vancouver, BC, Canada.
[7] da Silva, M. M., Bruls, O., Swevers, J., Desmet, W., and Van Brussel, H., 2009, "Computer-Aided Integrated Design for Machines With Varying Dynamics," Mech. Mach. Theory, **44**, pp. 1733–1745.
[8] Fonseca, P. D., 2000, "Simulation and Optimization of the Dynamic Behavior of Mechatronics Systems," Ph.D. thesis, Katholieke Universiteit Leuven, Leuven, Belgium
[9] Givoli, D., Barbone, P. E., and Patlashenko, I., 2004, "Which are the Important Modes of a Subsystem?," Int. J. Numer. Methods Eng., **59**, pp. 1657–1678.
[10] Litz, L., 1981, "Order Reduction of Linear State-Space Models via Optimal Approximation of the Non-Dominant Modes," Large Scale Syst., **2**, pp. 171–184.
[11] Feliachi, A., 1990, "Identification of Critical Modes in Power Systems," IEEE Trans. Power Syst., **5**, pp. 783–787.
[12] Shabana, A., and Wehage, R. A., 1983, "Variable Degree-of-Freedom Component Mode Analysis of Inertia Flexible Mechanical Systems," ASME J. Mech. Des., **105**(3), pp. 371–378.
[13] Tayeb, S., and Givoli, D., 2011, "Optimal Modal Reduction of Dynamic Subsystems: Extensions and Improvements," Int. J. Numer. Methods Eng., **85**, pp. 1–30.
[14] Park, K. C., and Park, Y. H., 2004, "Partitioned Component Mode Synthesis via a Flexibility Approach," AIAA J., **42**, pp. 1236–1245.
[15] Jakobsson, H., Bengzon, F., and Larson, M., 2011, "Adaptive Component Mode Synthesis in Linear Elasticity," Int. J. Numer. Methods Eng., **86**, pp. 829–844.
[16] Farhat, C. G., and Geradin, M., 1994, "On a Component Mode Synthesis Method and Its Application to Incompatible Substructures," Comput. Struct., **51**, pp. 459–473.
[17] Heirman, G., and Desmet, W., 2010, "Interface Reduction of Flexible Bodies for Efficient Modeling of Body Flexibility in Multibody Dynamics," Multibody Syst. Dyn., **24**, pp. 219–234.
[18] Liu, G. R., and Quek, S. S., 2003, *The Finite Element Method: A Practical Course*, Butterworth-Heinemann, Burlington, MA.
[19] Craig, R. R., Jr., and Bampton, M. C. C., 1968, "Coupling of Substructures for Dynamics Analyses," AIAA J., **6**, pp. 1313–1319.
[20] Guyan, R. J., 1965, "Reduction of Stiffness and Mass Matrices," AIAA J., **3**, p. 380.
[21] O'Callahan, J. C., 1989, "A Procedure for an Improved Reduced System (IRS) Model," Proceedings of 7th IMAC, pp. 17–21.
[22] Friswell, M. I., Garvey, S. D., and Penny, J. E. T., 1995, "Model Reduction Using Dynamic and Iterated IRS Techniques," J. Sound Vib., **186**, pp. 311–323.
[23] Koutsovasilis, P., and Beitelschmidt, M., 2010, "Model Order Reduction of Finite Element Models: Improved Component Mode Synthesis," Math. Comput. Model. Dyn. Syst., **16**, pp. 57–73.
[24] Ewins, D. J., 2000, *Modal Testing: Theory, Practice, and Application*, Research Studies Press, Baldok, Hertfordshire, UK.
[25] Chen, G., 2001, "FE Model Validation for Structural Dynamics," Ph.D. thesis, Imperial College of Science, Technology & Medicine, University of London, London.
[26] Cao, Y., and Altintas, Y., 2004, "A General Method for the Modeling of Spindle-Bearing Systems," ASME J. Mech. Des., **126**(6), pp. 1089–1104.
[27] ANSYS V12, 2009, Documentation for ANSYS.
[28] Altintas, Y., and Budak, E., 1995, "Analytical Prediction of Stability Lobes in Milling," CIRP Ann., **44**, pp. 357–362.
[29] Zulaika, J. J., Campa, F. J., and Lopez de Lacalle, L. N., 2011, "An Integrated Process–Machine Approach for Designing Productive and Lightweight Milling Machines," Int. J. Mach. Tools Manuf., **51**, pp. 591–604.